Measurement of Strain in Fabrics under Ballistic Impact using Embedded Nichrome Wires. Part II: Results and Analysis

Sidney Chocron, Charles E. Anderson, K. Ranjan Samant, Eleonora Figueroa, Arthur E. Nicholls, James D. Walker

Accepted Manuscript

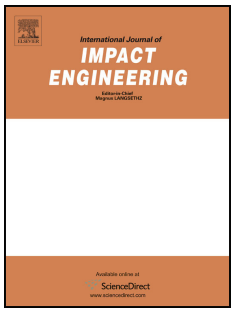

Title: Measurement of Strain in Fabrics under Ballistic Impact using Embedded Nichrome Wires. Part II: Results and Analysis

Authors: Sidney Chocron, Charles E. Anderson Jr.K. Ranjan Samant, Eleonora Figueroa, Arthur E. Nicholls, James D. Walker

PII: S0734-743X(09)00107-9

DOI: 10.1016/j.ijimpeng.2009.05.012

Reference: IE 1794

To appear in: *International Journal of Impact Engineering*

Received Date: 28 December 2007

Revised Date: 21 May 2009

Accepted Date: 27 May 2009

Please cite this article as: Chocron S, Anderson CE, Samant KR, Figueroa E, Nicholls AE, Walker JD. Measurement of Strain in Fabrics under Ballistic Impact using Embedded Nichrome Wires. Part II: Results and Analysis, International Journal of Impact Engineering (2009), doi: 10.1016/j.ijimpeng.2009.05.012

Measurement of Strain in Fabrics under Ballistic Impact using Embedded Nichrome Wires. Part II: Results and Analysis

Sidney Chocron*, Charles E. Anderson Jr., K. Ranjan Samant+
Eleonora Figueroa, Arthur E. Nicholls, James D. Walker

Southwest Research Institute, 6220 Culebra Rd., San Antonio, TX, 78238

+DuPont™ Central Research & Development, Experimental Station

P.O. Box 80304, Wilmington, DE 19880-0304

May 21, 2009

Abstract

A new technique using nickel-chromium wire, called the NiCr (Nichrome ®) wire technique, has been presented in a first paper describing the technique [1]. This second paper focuses on the results obtained when this new technique is applied to ballistic fabrics. Strain distributions on the layer impacted, as well as in different layers, are presented. An energy balance based on the strains is shown to provide reasonable values for the elastic energy stored by the yarns. Failure times of the first layer as a function of impact velocity are discussed and a simple momentum balance is shown to predict well the deflection history of the fabric. Ultra-high-speed photography and high-speed videos allowed recording of fabric deflection vs. time. The combination of the four diagnostic techniques, including X-rays, delivers a very complete picture of the impact mechanics in fabrics, both for early-time and late-time phenomena.

Keywords: Nickel-chromium (NiCr) wire, Kevlar fabric, ultra-high speed photography, high-speed video, Strain in fabric.

*Corresponding Author, S. Chocron, Southwest Research Institute, email: schocron@swri.edu

1 Introduction

A new technique using nickel-chromium wire, called the NiCr wire technique, has been developed to measure yarn strains in a fabric subjected to ballistic impact. Details of the technique are described in [1]. This paper focuses on using the technique, combined with a variety of other diagnostic techniques (flash radiography, high-speed video, and ultra-high-speed imaging), to study the response of ballistic fabric to impact.

The work relies on Smith's work [2] that described how the longitudinal and transverse wave move in a yarn impacted transversely. Roylance [3] and Cunniff [4]-[9] subsequently developed models that described qualitatively and quantitatively the motion and strain in a fabric under normal impact. A more complete bibliography is given in Ref. [1].

The yarns that form a cross in the fabric and are directly impacted by the projectile are know as the primary yarns. The secondary yarns are all the other yarns of the fabric. The NiCr wire technique, as used in this work, only allows measuring strains in secondary yarns. A direct impact on the NiCr wire breaks it instantly, and therefore, it does not provide any useful information other than a zero (impact) time.

The first part of this paper describes the materials and experimental technique succinctly. Then the local and global strain distributions obtained for the specific layer arrangement studied are presented as a function of the distance to the impact point and as a function of the layer number. An energy balance and momentum balance follow and are used to confirm that the strains measured are consistent with what is expected. Arrival and failure times of individual layers are also inferred from the NiCr wire data. Finally, deflection vs. time responses, including failure times, are obtained from analysis of high-speed video and ultra-high speed images.

2 Materials and Methods

2.1 Ballistic Fabric and Projectile

The ballistic tests were performed on targets with 22 layers of Kevlar® 129 (Style S726) with 840 denier yarns (areal density of the 22 layers target 4.40 Kg/m^2). The targets were provided by Du Pont^{TM}. The size of the targets was 43.2 $cm \times 43.2$ cm but the targets were placed inside an aluminum frame with a square opening of

30.5 $cm \times 30.5$ cm. The torque applied on all the bolts for all the tests was 27 Nm. The projectile used was a .357 Magnum, 158 grain (10.24 gram) jacketed soft point (JSP), with a diameter of 9.07 mm (0.357 in), and length 16.9 mm (0.67 in). Only one shot per target was performed, always in the center of the target. Figure 1 provides a schematic of the experimental set-up, along with various diagnostic equipment.

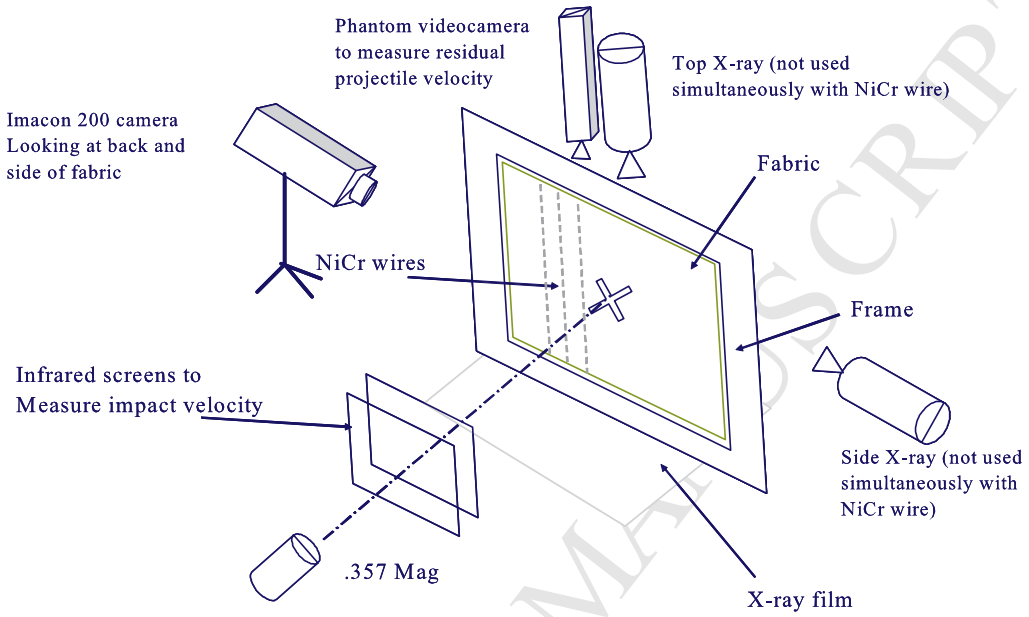

Figure 1: Schematic of the test set-up

2.2 Diagnostics

- **Infrared screens.** Infrared screens provide trigger signals whenever the screens detect the projectile blocking the light from the emitter to the detector. The signals are input into a counter that gives the time the projectile took to travel from the first to the second screen. The second screen was used to trigger all other diagnostic systems. These screens gave very consistent impact velocities.
- **Phantom high-speed video camera.** A Phantom V7 camera was used to measure the residual velocity of the projectile. The camera records images of the projectile after going through the target. The frame rate was one frame every 64 μs with a the resolution 800×240. The camera recorded the deflection of the back of the target. The camera images were calibrated for quantitative measurements by using a calibration bar aligned with a laser inserted in the gun barrel. The information obtained with this diagnostic was: 1) residual velocity of the projectile, 2) late-time deflection of fabric and pyramid base.

- **Imacon 200 ultra-high-speed photographic camera.** The Imacon camera takes a maximum of 16 frames at a maximum rate of one every 5 ns. The resolution per image is 1200×980 pixels. This camera was used to look at the back and side of the target (using a mirror to split the image) during the first 50-80 μs, taking one frame every 5 μs. The exposure used was 800 ns. The area observed was 6 $cm \times 6$ cm. To be able to measure distance in the frame, the plane of the bullet was calibrated using a ruler and a laser (for alignment). The information obtained from the Imacon images was: 1) position and speed of the transverse wave in the fabric, 2) position and speed of the apex of the pyramid, 3) time it takes the transverse wave to reach the NiCr wires, and 4) time of perforation of the last layer.

- **Orthogonal X-ray shadowgraphs.** Orthogonal X-ray heads were positioned to the side and above the target. Both heads were used in the same test but with delay between the images to obtain a sequence of X-ray histories of the impact. The heads were used at 22 keV with digital films that do not need to be chemically developed. The digital films were scanned directly to a PC allowing fast turnover and high resolution. The information obtained from the X-ray images was: 1) shape of the projectile while inside the target, 2) images of the inside of the target, including layer failure, layer motion, etc. (The X-rays could not be utilized simultaneously with the NiCr wire because of electromagnetic interference. They were also not used simultaneously with the Imacon camera because the X-ray film holder interfered with the line-of-sight to the Imacon.)

- **NiCr wires.** The NiCr wire technique is described in [1]. The NiCr wires constitute one of the arms of a Wheatstone bridge (120 Ω). The wires were calibrated through three initial tests where a strain per volt was determined. Each wire was shunted with a 5 KΩ resistance before the test to find its specific calibration factor. The digital data acquisition system had 8 channels and a maximum rate of 1 MHz. When using four channels or less, the sampling rate was 5 MHz. The information inferred from the NiCr wires was: 1) local strain of the yarn during the first few microseconds after impact, 2) global strain of the yarn during late-time response.

3 Analysis of the Data from the NiCr Wire Technique

3.1 Introduction

When a projectile impacts a fabric target, momentum and energy are transferred from the projectile to the fabric. The energy of the projectile goes, mainly, into kinetic and strain energy of the fabric, although other possible "sinks" of energy could be friction (layer/layer, yarn/yarn, projectile/yarns), generation of free surfaces (failure of yarns), plastic deformation of the projectile (heat) , etc.

It is now possible, using the NiCr wire technique, to estimate quantitatively how much energy is absorbed in straining the fabric. Of course, the strain in the fabric depends on time and position, and the NiCr wire technique is limited to very early time or very late time [1]. Nevertheless, the information that can be obtained can improve our understanding of what is happening in the fabric at the yarn level, as well as provide results useful for validation of numerical or analytical models.

First, the dependence of the strain with layer number will be presented, both at the local and global level. "Local" is used in this paper to mean "during the first few microseconds", when the yarn has only deformed locally because the wave has not had time to travel to the boundary. "Global" is used for deformations that happen at late times ($\sim 1000\ \mu s$ or more), i.e., the strain waves have had time to travel back and forth from the boundaries multiple times. The second analysis will present the variation of strain along one of the layers of the fabric.

3.2 Strain distribution as a function of the layer number

3.2.1 Local Strain

Local strain in the fabric was inferred from the equation derived in [1] that relates local strain with the slope of the signal of the NiCr wire:

$$\epsilon_0 = \frac{k_w \alpha}{2 c_{fab}} \tag{1}$$

where ϵ_0 is the strain in the yarn, k_w a calibration coefficient, α is the initial slope of the voltage vs. time curve, and c_{fab} the sound speed in the fabric. The individual signals were analyzed for every test configuration. Figure 2 shows the strain inferred for different impact velocities as a function of layer number for NiCr wires placed at

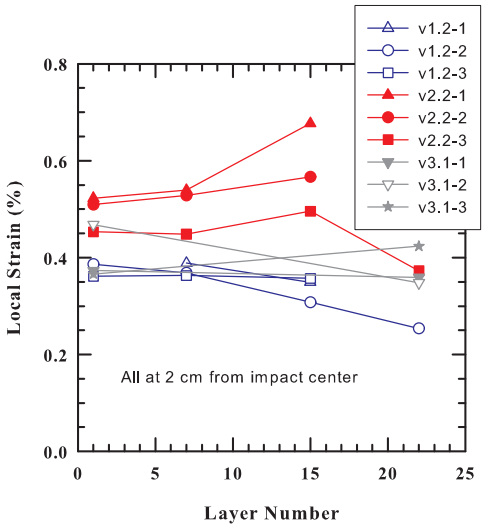

Figure 2: Dependence of local strain (at 2 cm from impact point) with layer number for different impact velocities.

a distance of 2 cm from the impact center. V1.2-2 is an example of test with four NiCr wires, all placed 2 cm away from the impact point and in layers 1, 7, 15 and 22. Layer 1 is the first layer the projectile impacts, layer 22 the last layer. All the tests named "V1" have, nominally, the same impact velocity, 360 m/s, although the real impact velocity varied slightly from test to test. All the projectiles in test series V1 were stopped with perforation of only one or two layers. The tests named "V2" had a nominal velocity of 500 m/s, 50 m/s above the ballistic limit; and the "V3" velocity was 450 m/s, very close to ballistic limit.

As expected, the local strains are higher at higher impact velocities. The strains from the different experiments at nominally the same impact velocity were averaged, and these averages are plotted in Fig. 3. We note that there is only one data point in that figure for layer 22.

There are two important aspects to point out in Fig. 3. First the magnitude of the strains are around 0.5% for the higher velocity impacts and 0.4% for the lower velocity impacts. Both Cunniff [9] and Roylance [3] show strains in *principal* yarns to be around 1.5% or 2%, but no published data were found for *secondary* yarns. Nevertheless, it will be shown that the strains measured with the NiCr wire are consistent with an energy balance (Section 3.4). The second important feature in Fig. 3 is that the strain does not seem to decrease (or increase) sharply with the layer number. This means that all the layers are experiencing similar strains (although for

the same radial distance from the impact point, layer 15 will see the strain sligthly later in time than layer 1, for example). The implication is that the strain in the first and last layer of a target, in this configuration, is very similar, although there appears to be a trend for slightly smaller strains in layer 22. Novotny [10], using a numerical model, reported a similar trend, and similar strains to those measured here experimentally, for an 8-ply fabric system.

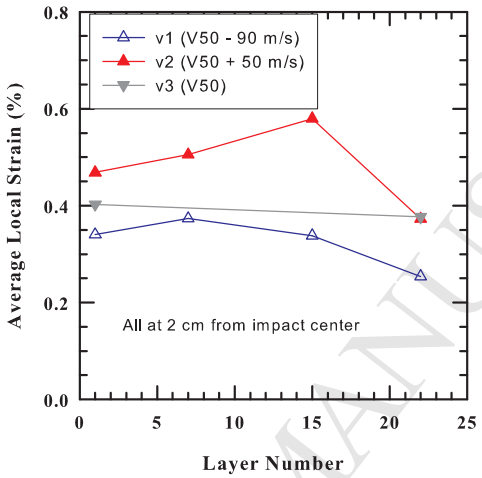

Figure 3: Dependence of local strain with layer number for different tests. The strains shown in Fig. 2 were averaged for each of the three nominal impact velocities.

3.2.2 Maximum Global Strain

Global strains are calculated using the NiCr wire as a long strain gage, i.e. it is assumed that the strain is uniform along its whole length. In that sense only an "average" strain is being obtained with this technique. Since no data of this kind can be found in the literature it is thought to be of interest. The following equation, derived in [1], was used to calculate global strain.

$$\epsilon = 1.41\% \frac{\Delta V_w}{\Delta V_{sh}} \tag{2}$$

where ΔV_w is the drop in voltage in the NiCr wire and ΔV_{sh} is the drop in voltage in the shunt resistance. The global strain, as opposed to the local strain, depends on the time; therefore, attention is focused on the *maximum* global strain achieved during the entire impact event, i.e., the strain at maximum deflection.

Figure 4 shows the "late-time" signal recorded with the NiCr wire. All the wires were placed in layer 1. By late-time it is meant the signal is recorded up to 10,000 μs.

These signals have been smoothed by averaging ten points to make the files easier to handle with the available software. So, although the sampling rate was 1 MHz, the averaging process changes the effective rate to 0.1 MHz.

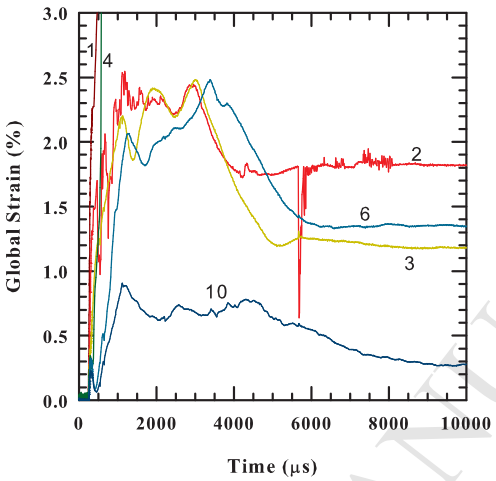

Figure 4: "Late-time" signal recorded with the NiCr wires for test V1.1-1. The NiCr wires were all placed in layer 1. The numbers of the legend represent the nominal distance in cm from the impact point.

Out of the nine wires used in test V1.1-1, four gave late time information, Fig. 4. Wires 1 and 4 failed in the early phase, the reason being unclear. The plot conveys that the maximum strain that the wires measure occurs sometime between $t \sim 1000\ \mu s$ and $t \sim 3000\ \mu s$. The Phantom cameras (see Section 5) confirm that maximum deflection of the fabric also happens in the same time frame. After going through the maximum, the fabric springs back but the NiCr wire strain does not go back to zero. The reason is probably that the wire has undergone some amount of plastic deformation (since according to the NiCr wire stress-strain curve, [1], the wire material undergoes plastic deformation for strains greater than 1%). Although strains were measured for longer times ($t \sim 90,000\ \mu s$), these strains were always less than the maximum strains ($t \sim 1000 - 3000\ \mu s$) and were not useful in providing further insights.

Figure 5 shows the average, for each impact velocity, of the maximum global strain for the different layers. Only wires at 2 cm from the impact point were used to create this plot. Again it is apparent that the strain does not seem to depend on the layer number since it is pretty uniform across the target. The maximum strains are on the order of 0.5 to 2.5% and, as expected, the maximum global strains are smaller

for higher impact velocities. As the analysis of the Phantom camera will show (as well as postmortem observations), deflection is much smaller when fabric perforation occurs. Less energy/momentum is transferred to the target at high velocities because there is less time for projectile/fabric interaction since the fabric fails rapidly. The result is that less deflection and strain are produced above the ballistic limit than below the ballistic limit.

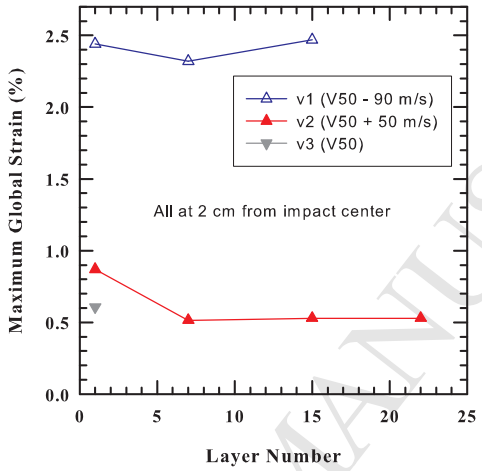

Figure 5: Dependence of maximum global strain (late time) with layer number for different tests

3.3 Strain distribution as a function of the distance to the impact point

3.3.1 Local Strain

The strain distribution across the layer, during ballistic impact, is of great interest since it helps understanding how a fabric functions, the distribution of energy and, eventually, improving fabric performance. Again it is difficult to find in the literature strain data distribution in a fabric layer other than Roylance [11], although numerical models (like the ones developed by Duan [12], Shahkarami [13], G. Johnson [14]) or analytical models (Gu [15], Walker [16], Pankaj [17]) should in principle provide the strain everywhere in the fabric.

Figure 6 shows that the strain decreases as distance from the impact point increases, as expected. It also shows that the local strain at impact velocities of 500 m/s

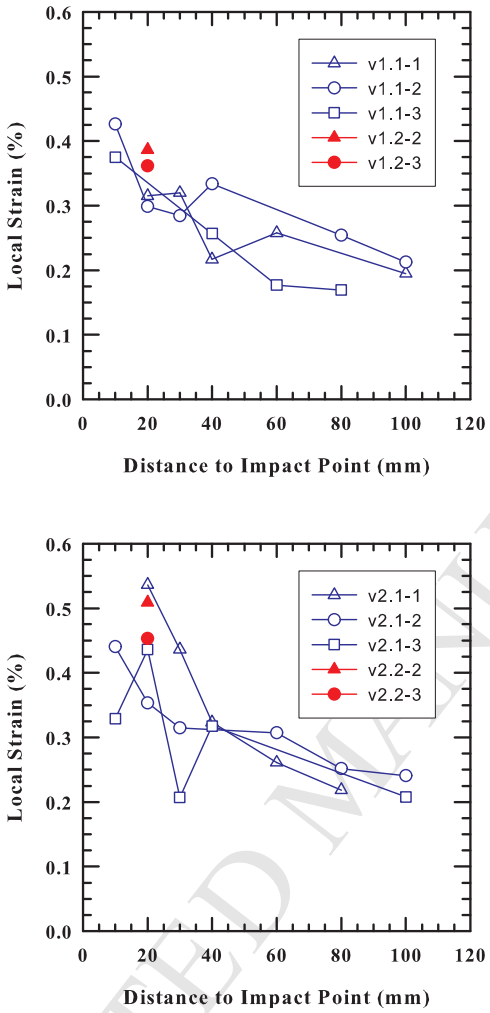

Figure 6: Local strain distribution as a function of the distance to the impact point. a) Impact velocity V1=360 m/s b) V2=500 m/s

is only slightly larger than at 360 m/s. This implies that, the secondary yarns react similarly to a perforating and to a non-perforating impact during the first few microseconds after impact. Figure 7 is the average, for each impact velocity, of the data shown in Fig. 6. The data from all layers were used during averaging since the layer number did not seem to play a major role. As already indicated, these averages show that local strains are slightly larger for the higher impact velocity, but they differ only by $\sim$ 0.1% . The data in Fig. 7 also indicates that the local strain "far" from the impact point ($\sim$60 mm or more) asymptotes to approximately 0.20%. The V2 (10 mm) datum seems to be an anomaly, maybe influenced by the failure of the layer.

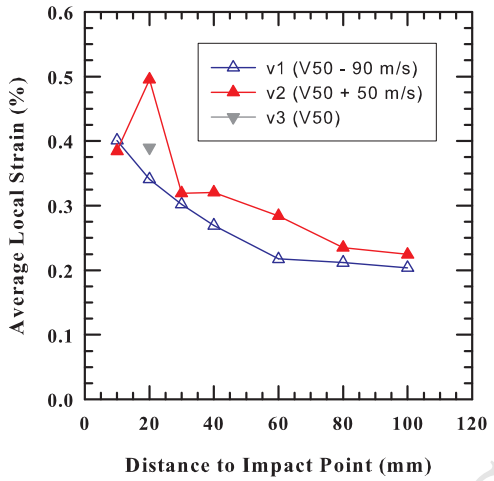

Figure 7: Average local strain distribution as a function of the distance from the impact point. (These are averages of the data shown in Fig. 6)

3.3.2 Maximum Global Strain

Maximum global strain results should, in principle, be very different from local strain. The fabric has much more time to deflect and strain the yarns. Also, camera images and experience show that at high impact velocities, when full perforation occurs, deflection of the fabric is much smaller than when the impact happens at a velocity close to the ballistic limit. In fact, Kevlar® fabric absorbs much more energy from the projectile right below the ballistic limit than above it. This was observed by Cunniff [8] and corroborated in this project. As mentioned above, maximum global strain occurs generally around t$\sim$ 2000 μs. The maximum global strains as a function of distance from the impact point are plotted in Fig. 8.

The global strains vary between $\sim$ 2.5% and $\sim$ 0.75% for the impact velocity 90 m/s below V50, Fig. 8(a). The large differences between the two experiments may be due to differences in slippage of the fabric and NiCr wire at the boundary [1]. The maximum global strains at the impact velocity 50 m/s above V50 show a trend that the global strains decrease with distance form the impact point. It is recognized that is a lot of scatter in the global strain measurements in a limited number of experiments. It is therefore appropriate to look at the averages of the two impact velocities, Fig. 9, and examine the trends. It is observed that the global strain decreases with distance from the impact point. As expected, the strains measured at high impact velocities (above the ballistic limit) are smaller than those below the ballistic limit. The global strain in the fabric is larger for the lower impact velocity

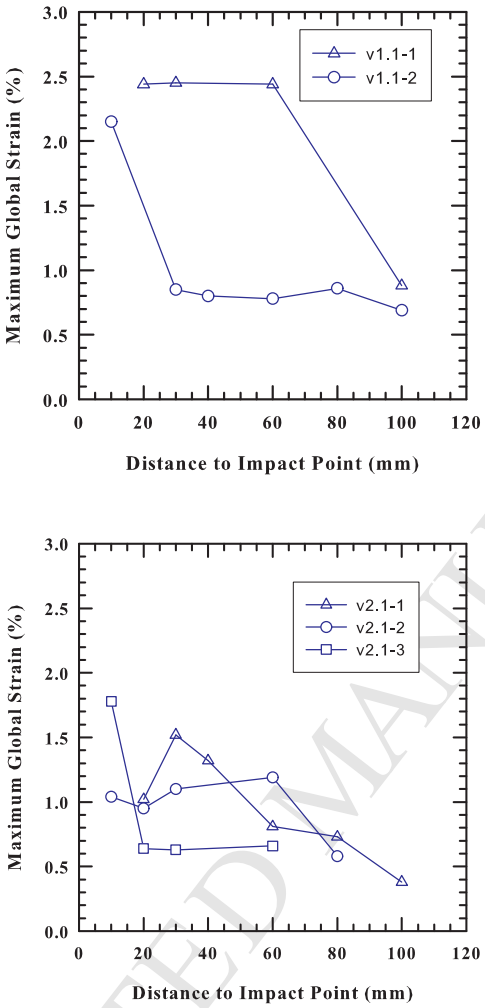

Figure 8: Maximum global strain distribution as a function of the distance from the impact point. a) Impact velocity V1=360 m/s b) Impact velocity V2=500 m/s

at every point with the exception of the one at a distance of 40 mm, where only one experimental point is available. This point, where the strains unexpectedly cross each other, is assumed to be an artifact due to the nature of averaging process.

3.4 Energy balance

3.4.1 Introduction

Conservation of energy is a very intuitive but rather difficult physical quantity to use in ballistic impact studies. The problem is that energy can take many "forms" and it is sometimes difficult to evaluate where the energy is going. Nevertheless it was

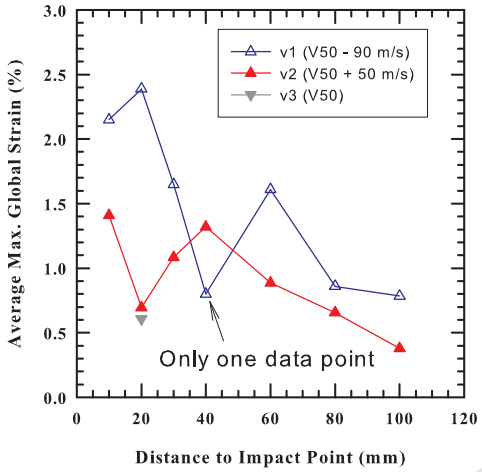

Figure 9: Average of maximum global strain distribution as a function of distance from the impact point.

decided to do an energy balance for the different tests to evaluate the consistency in the strain numbers obtained with the NiCr wire. The initial kinetic energy of the projectile (before contacting the target) should go to one of the following "sinks": 1) strain of the fabric ($\mathcal{E}_{str}$), 2) deformation of the projectile ($\mathcal{E}_{def\ p}$), 3) friction between projectile and fabric ($\mathcal{E}_{frict\ p-f}$), 4) yarn-yarn or layer-layer friction ($\mathcal{E}_{frict\ y-y}$), 5) kinetic energy of fabric ($\mathcal{E}_{kin\ f}$), 6) kinetic energy of residual projectile, and 7) failure of yarns ($\mathcal{E}_{fail\ y}$). Even this "long" list has neglected some terms like failure of projectile, energy absorbed by the frame, etc. The following equation expresses the list in mathematical terms:

$$\mathcal{E}_{lost\ p} = \mathcal{E}_{str} + \mathcal{E}_{def\ p} + \mathcal{E}_{frict\ p-f} + \mathcal{E}_{frict\ y-y} + \mathcal{E}_{kin\ f} + \mathcal{E}_{fail\ y} \tag{3}$$

where $\mathcal{E}_{lost\ p}$ is the energy lost by the projectile, i.e. the difference between the initial and residual kinetic energies.

It is straightforward to show that the energy required to deform the projectile is negligible compared to the total energy lost, which is on the order of $\mathcal{E}_{lost\ p} \sim 500\ J$. The projectile is made of a lead core so the yield strength is ~10 MPa. The plastic work needed to reduce the length of the projectile from L_0 to L is given by:

$$W = \int_{L_0}^{L} Y A(L) dL \tag{4}$$

where it is assumed that strength, Y, is constant and the cross section, A, varies but

the volume is constant. Then:

$$W = Y \int_{L_0}^{L} \frac{V}{L} dL \tag{5}$$

where V is the volume of the projectile. Integrating this equation gives:

$$W = YVln\frac{L}{L_0} \approx 7\ J \tag{6}$$

where $V \sim \pi \times 9^2/4 \times 16 \sim 1000\ mm^3$, and the final length was assumed to be half of the initial length. So, since $W \ll \mathcal{E}_{lost\ p}$, the plastic work energy will be ignored.

A similar argument can be used to ignore the energy needed to fail the yarns. That elastic energy is:

$$\mathcal{E}_{fail\ y} = \frac{1}{2} ALE\epsilon_{fail}^2 \tag{7}$$

where A is the cross section of the yarn, L its length, E its elastic modulus, and ϵ_{fail} is the strain to failure of the yarn. The cross-sectional area of a yarn is 0.0525 mm^2, and its elastic modulus is 99.1 GPa. Strain to failure for a yarn is 3.25%. If it is assumed that maximum strain is localized in an area of 3 diameters around the projectile (a conservative assumption) then:

$$\mathcal{E}_{fail\ y} = .5 \times 0.0525\ mm^2 \times 6 \times 9\ mm \times 99.1\ GPa \times 0.0325^2 \sim 0.15\ J \text{ per yarn} \tag{8}$$

Since there are 22 layers and around 10 yarns per layer that fail, the energy needs to be multiplied by 220 giving $\sim 33\ J$ for the energy lost because of failure. Again this energy is very small compared to the total energy lost by the projectile, particularly since a very large distance was assumed for the maximum strain.

The energy going to friction between projectile and fabric will be assumed to be small without any experimental arguments. It is noted, though, that the numerical work presented by Duan [18] seems to show that it could have some influence. In summary it is possible to write the energy balance, ignoring negligible terms, as:

$$\mathcal{E}_{lost\ p} = \mathcal{E}_{str} + \mathcal{E}_{frict\ y-y} + \mathcal{E}_{kin\ f} \tag{9}$$

This equation will be used in the sections below.

3.4.2 Energy lost by the projectile during penetration

The tests to determine the ballistic limit of the fabric were performed before any of the instrumented tests. The setup for the V50 tests was the same with respect to the frame and torque grip on the fabric. The four-shot ballistic limit, calculated from the first four lines in Table 1 was 446 m/s. The spread was 16 m/s.

Test #	V(m/s)	Result
1	439	No perforation
5	435	No perforation
6	454	Perforation
4	455	Perforation
3	486	Perforation
2	502	Perforation
V50	446	

Table 1: Tests performed on targets to find the ballistic limit.

The average energy absorbed for the different impact velocities is listed in Table 2. All the energy was absorbed for the tests at velocities V1 and V3 since the projectiles were stopped within the fabric. For the overmatched condition (V2), the residual velocity of the bullet after perforating the fabric was 386 m/s.

Tests	Avg. Initial Kin. Energy (J)	Avg. Energy Absorbed (J)
V1∼360 m/s	679	679
V2 ∼500 m/s	1280	515
V3∼450 m/s	1014	1014

Table 2: Average energy absorbed by the fabric at the different impact velocities.

3.4.3 Energy balance at projectile arrest for V1

The energy equation (9) can be used at any instant during the penetration process. In this section the strain energy in the fabric will be evaluated at the instant of maximum deflection by using the "average" global strains measured from the NiCr wires. Only the V1 impact velocity is considered in this section. Assuming the slippage at the edge of the frame is negligible, maximum deflection and maximum global strain should occur simultaneously. At maximum deflection the kinetic energy of the fabric is very small since only in-plane motion is possible. Consequently, the kinetic energy

of the fabric will be assumed to be negligible at maximum deflection.

The strain energy stored in a single yarn, assuming the strain is uniform along the yarn is given by:

$$\mathcal{E}_y = \frac{1}{2} ALE\epsilon^2 \tag{10}$$

the symbols have the same definition as for Eq. 7 and ϵ is the strain. Since the NiCr wires give the strain distribution at some specific distances from the impact point, a smooth exponential curve fit was performed to the strain distribution, see Fig. 10:

$$\epsilon(x) = 2.0402\ e^{-0.0098x} \tag{11}$$

This exponential is a curve fit for strains measured in a range of distances between 10 and 100 mm from the impact point. The strain is extrapolated from the same equation for distances smaller than 10 mm or larger than 100 mm (the maximum distance in the frame is 150 mm) . Equation 11 provides an estimate of the strain everywhere in the fabric so the strain energy can be calculated for any single yarn in the fabric.

Figure 10(b) shows the strain energy for a single yarn of the fabric as a function of the distance of the yarn to the impact point. Since the number of yarns in the fabric is $\sim$26 per inch, the distance in mm also corresponds approximately to the yarn number. The strain energy for a single yarn in the fabric as a function of distance from the impact point is found from Eqns. (10) and (11), with $L = 304.8\ mm$. This strain distribution is shown in Fig. 10(b). Summing the strain energy per layer over the 612 yarns in a layer gives the total strain energy stored in a single layer: 73.20 J. Assuming the strain is similar in all 22 layers (as shown by the NiCr wires), the total strain energy stored in the target is: 1610 J, more than double the 679 J absorbed in average (Table 2) by the fabric for an impact velocity of 360 m/s. Fig. 10(a) also shows, as a dashed line, the strain "required" to match the correct energy of the projectile. The curve fit used for the dashed line was:

$$\epsilon(x) = 1.42\ e^{-0.0098x} \tag{12}$$

This curve suggests that we are overestimating the strain by around 0.5-0.7% strain, an error similar to the one estimated in [1] for slippage in the frame. It is interesting to note that a small change in the strain distribution results in a large difference for the energy absorbed.

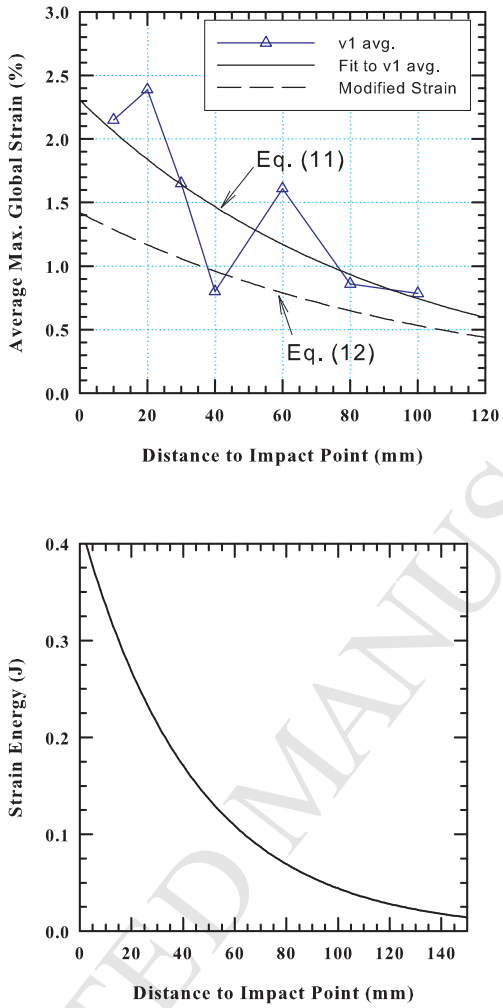

Figure 10: a) Curve fit to the maximum global strain measured with the NiCr wires. The dash line indicates the strain "needed" to correctly match the energy of the projectile. b) Strain energy as a function of distance to impact point using Eqns.(10-11)

3.4.4 Energy balance at maximum deflection for V2

The same procedure was used to perform the energy balance at maximum deflection for impact velocities of 500 m/s. The equation fit is now:

$$\epsilon(x) = 1.1994\ e^{-0.0092x} \tag{13}$$

Adding the energy for the 612 yarns using the above equation gives the total strain energy stored in the target: 643 J. In this case the enery balance is only 20% larger than the energy lost by the projectile. The energy error translates, in terms of strain,

in very small errors on the order of 0.1% or less, as seen in Fig. 11, where the strain distribution that gives the 515 J (Table 2) is shown together with the exponential fit to the strain measured in the tests.

As mentioned in [1], for impact velocities of 500 m/s the slippage on the frame was observed to be minimal. This reduces the error of the NiCr wire measurements since the gage length stays constant throughout the whole experiment. One way to show that slippage is minimal for this high-velocity experiment is to examine the time frame of the dynamics. The wave takes $\sim \frac{0.3048\ m}{2\times5500\ m/s} \sim 28\ \mu s$ to reach the frame. The fabric is perforated at $\sim 50\ \mu s$. Therefore, motion of the yarn at the boundary has very little time to develop before the release waves arrive (motion in the plane of the fabric is very slow), and thus, slippage is minimal.

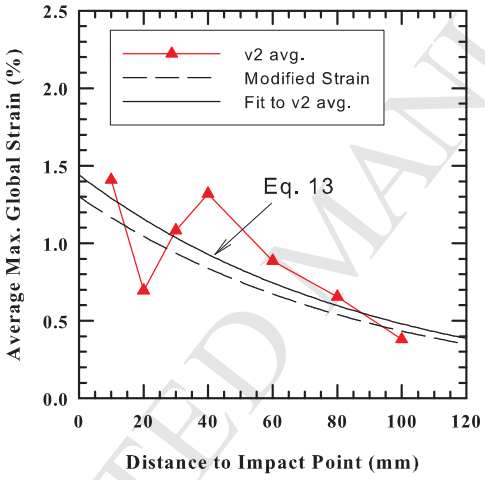

Figure 11: Curve fit (continuous line) to the maximum global strain measured with the NiCr wires for velocity V2=500 m/s. The dashed line shows the strain distribution needed to match the (average) energy lost by the projectile.

3.4.5 Energy balance at time of failure for V2

The energy equation can also be used at the time of full perforation ($\sim 50\ \mu s$, see Fig. 19) for an impact velocity above the ballistic limit. An added complication in this case is that the kinetic energy of the fabric is no longer negligible. The Imacon images were used to account for the kinetic energy of the fabric. The strain energy was calculated with the measurements inferred from the NiCr wires. For this energy balance, the "local" strain, which is valid only for early time, was used.

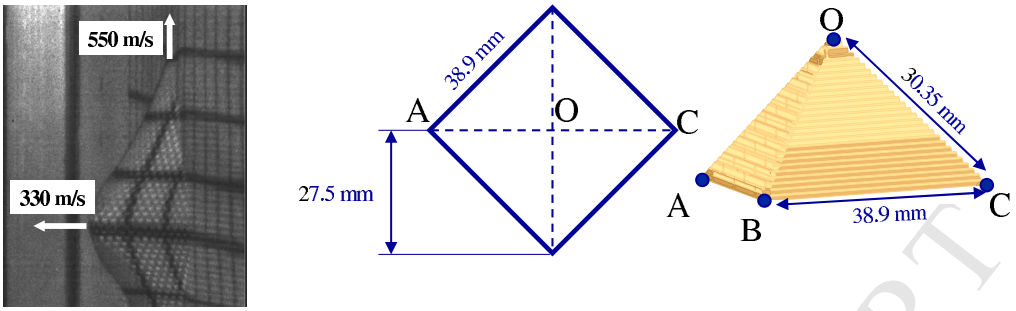

Figure 12: a) Pyramid and velocity field measured with the Imacon b) Pyramid geometry used in the energy balance.

To calculate the kinetic energy of the fabric at the instant of full penetration the velocity of the apex and base of the pyramid were measured from the Imacon images. Section 4.1 provides the details about these measurements. The apex was determined to be moving at 330 m/s at failure and the base of the pyramid at 550 m/s, Fig. 12. Since the Imacon images indicate that full penetration takes $\sim 50\ \mu s$, then the semi-diagonal of the pyramid measures: $0.55\ km/s \times 50\ \mu s = 27.5\ mm$. The images also show, see Section 4.1, that the semi-angle ($\widehat{AOC}/2$) of the pyramid is 65 degrees. According to this geometry, the surface of one of the faces of the pyramid should be: $0.5 \times 38.9\ mm \times 23.3\ mm = 453\ mm^2$. The surface of the four faces for the 22 layers is then: $0.0399\ m^2$, and the mass of the pyramid $0.2\ kg/m^2 \times 0.0399\ m^2 = 7.97\ gram$. The kinetic energy of the pyramid is then: $\frac{1}{2}\left(7.97 \times 10^{-3}\ kg\right) 330^2 = 434\ J$.

To account for the strain energy at time of failure, a similar curve fit to the one presented in the previous section was performed. Figure 13 shows the curve fit for the local strain. The equation is:

$$\epsilon(x) = 0.4508\ e^{-0.0075x} \tag{14}$$

Using the curve fit to calculate the strain energy in the fabric gives a strain energy[1] of 86 J, only 20% of the energy lost by the projectile. But adding both the strain and fabric kinetic energy (434 J) gives 520 J, in excellent agreement with the energy lost by the projectile (515 J) given in Table 2.

It is important to point out that being able to account for all the energy of the bullet as kinetic and strain energy in the fabric does not mean that yarn to yarn friction is not an important mechanism. It just means that friction is an "effective"

[1]Note that this implicitly assumes that the strain wave reached the frame and the strain is constant in the whole yarn length L=30.48 cm

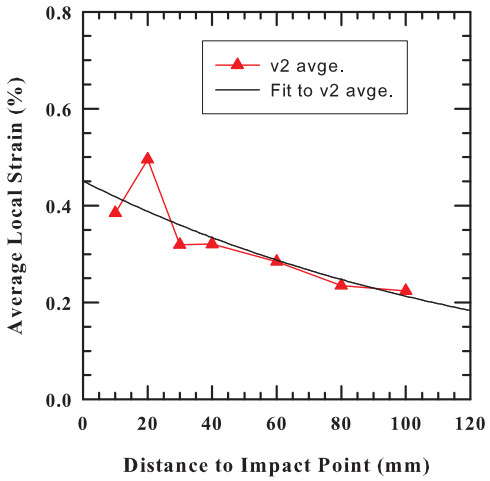

Figure 13: a) Curve fit to the local strain measured with the NiCr wires.

mechanism to transmit strain from one yarn to the other without dissipating energy in that transmission.

3.5 Arrival and failure times

An interesting question that can be addressed with the NiCr wire is how long, after the first layer is contacted by the projectile, does it take the other layers to "feel" that an impact has happened. Obviously, layer 22 will be the last layer to sense the impact, and the time elapsed from contact of the first layer to strain of the last layer should depend on the impact velocity. The NiCr wire was placed 2 cm from the impact point in four different layers through the target. Testing was done at the three impact velocities: 360 m/s (V1), 500 m/s (V2), and 450 m/s (V3). Figure 14(a) shows "arrival" times of the strain wave for the different layers. The first layer was used as the reference for time (i.e. arrival time at first layer is zero). The symbols in Fig. 14(a) are the data from the tests, the lines follow the average for each impact velocity and layer.

As expected, arrival times are longer for the lower impact velocity. Also, according to Fig. 14(a), it takes – on average – 30 μs more for the last layer to sense that an impact has happened in the front layer.

Figure 14(b) shows the time it takes the *first* layer to fail for two different impact velocities. The open symbols are the test data. The solid symbols represent the

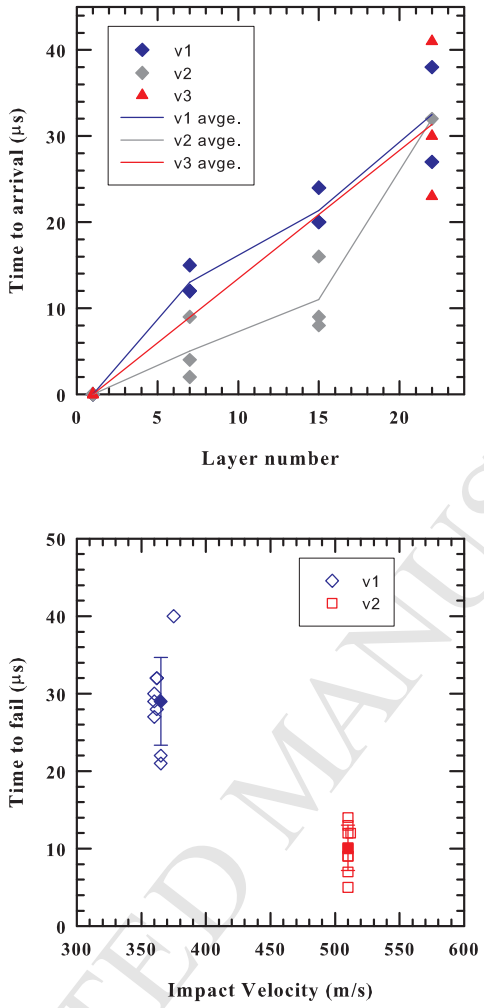

Figure 14: a) Arrival time of the longitudinal wave for the different layers at three impact velocities b) Failure time for the first layer as a function of impact velocity.

average and the error bars the standard deviation. The average failure time, from contact of the first layer, is $\sim 10\ \mu s$ at impact velocities of ~ 500 m/s. From camera images, it takes approximately 50 μs, from contact, for failure of the last layer. This means that the last layer survives on average 40 μs longer than the first layer. A possible explanation for this effect is that the last layer senses the impact, before being contacted by the bullet, through a compression wave transmitted by the layers behind. This gives more time for the last layer to begin moving and avoid being sheared by the projectile. Since the last layer is not constrained by layers behind, it is easier to start its motion.

From the above observation, it would seem that a target with more layers, but less areal density per layer (the total areal density remains the same), should perform better, at least in this particular configuration. The compressive wave that communicates strain from layer to layer seems to travel faster than the projectile and, the earlier the last layers know about the impact (compared to the time it takes the bullet to actually be in contact with the last layer) the better, since the last layers will have more time to initiate motion and "absorb" momentum from the projectile. From that perspective it would seem that "thicker is better" when comparing targets with the same areal density at these impact velocities. Actually this phenomenon has been recently observed and published by Broos [19].

4 Analysis of Early Time Data Taken with the Imacon Camera

4.1 Deflection vs. time and pyramid angle histories

The Imacon ultra-high-speed camera allows the user to measure distances and, with the time between images, velocities of the back face of the target can be calculated. Used for early times it shows the evolution of the waves before the waves have time to interact with the boundary and come back to the impact point. Careful alignment and parallax correction, as well as a distance calibration, were performed to ensure distances were properly measured in the plane of motion of the projectile. The estimated error in these measurements is ± 1 mm. The times were shifted to make t=0 the first frame showing a bulge.

Figure 15 is an example of the data obtained for all the tests at an impact velocity of V1=360 m/s. Both the base and the apex seem to move at approximately constant velocity, at least for the first 60 or 70 μs recorded by the Imacon camera. Linear fits to each data set gave correlation coefficients of 98% or better[1]. The average semiangle of the pyramid (at apex) is easily calculated from the height and semidiagonal. Figure 16 shows the evolution of the angle. The angle stays almost constant ($65^o - 70^o$) during the first 120 μs.

At higher impact velocities like V2 and V3 (respectively 500 and 450 m/s), the apex velocity as well as the base velocity (which is also the transverse wave velocity)

[1]We understand that fabric deflection vs. time is in reality not linear. However at early times a linear reponse appears to be a good approximation.

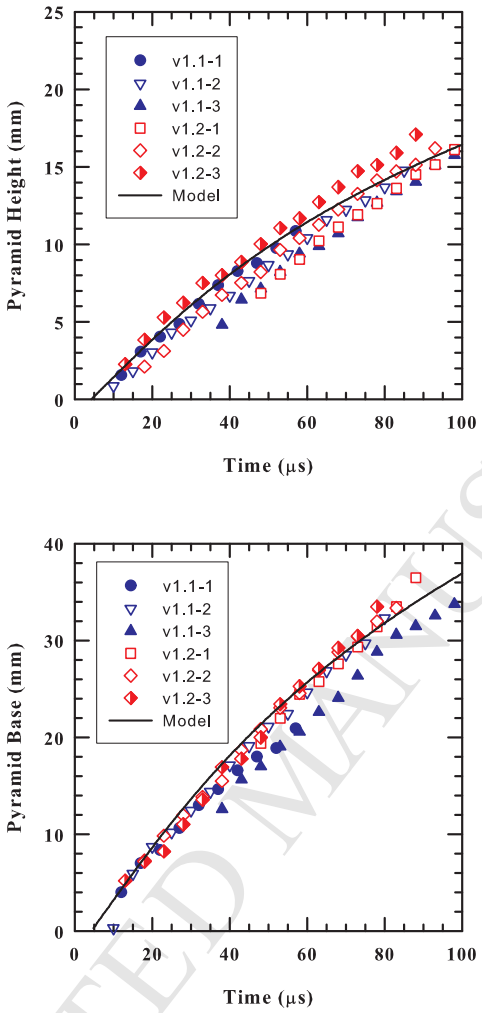

Figure 15: a) Height of the apex of pyramid vs. time as measured with Imacon for an impact velocity of 360 m/s b) Size of the semidiagonal of the base vs. time. The black lines are results from an analytical model that is presented in Section 4.3.

were also observed to be almost constant for this early-time range. However, there is a sudden change in slope for the apex and base position vs. time as soon as failure occurs. As expected, failure slows both the apex and the transverse wave quickly.

Figure 17 shows the average apex and transverse wave velocities for the different impact velocities (before failure). The error bars on the figure represent the standard deviation. As expected, apex and transverse wave velocity increase with impact velocity. On the other hand, the semiangle measured at the apex (Fig. 18) is approximately a constant, although there appears to be decreasing slightly at the

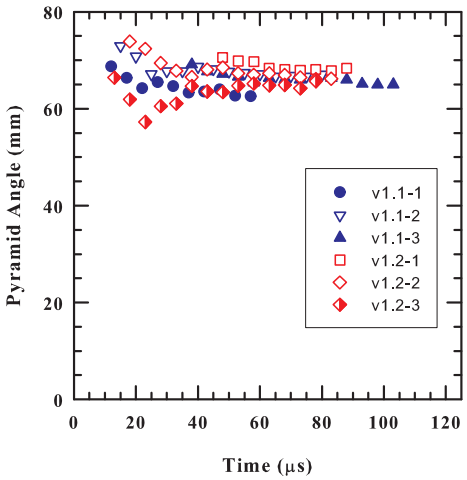

Figure 16: Semiangle of the pyramid at apex, inferred from height and semidiagonal.

highest impact velocity.

4.2 Failure times with Imacon

Failure times can also be measured with the images obtained from Imacon camera for impact velocities that resulted in perforation (V2=500 m/s). Fig. 19 shows failure of the back layer around $t \sim 50 - 55\ \mu s$ after the first appearance of bulging of the back layer.

Pyramid height and base semidiagonal for the tests performed at impact velocity V2∼500 m/s are shown (Fig. 20). Failure is difficult to identify in these plots, although there is a slight change in slope at around 55 μs in Fig. 20(b).

4.3 Momentum balance

The momentum lost by the projectile is transferred to the fabric, i.e.,

$$\frac{d(M_p V)}{dt} = -\frac{d(M_f V)}{dt} \tag{15}$$

where M_p is the mass of the projectile (constant), V its velocity, assumed to be the same as the apex velocity for the fabric, and M_f the mass of the fabric involved in the impact, which increases with time. The primary assumption, as has been demonstrated experimentally, is that the pyramid angle is constant (65 degrees). It is also assumed that the fabric has not been perforated, i.e., the projectile and apex of the pyramid are moving together. With these assumptions, the mass of the fabric

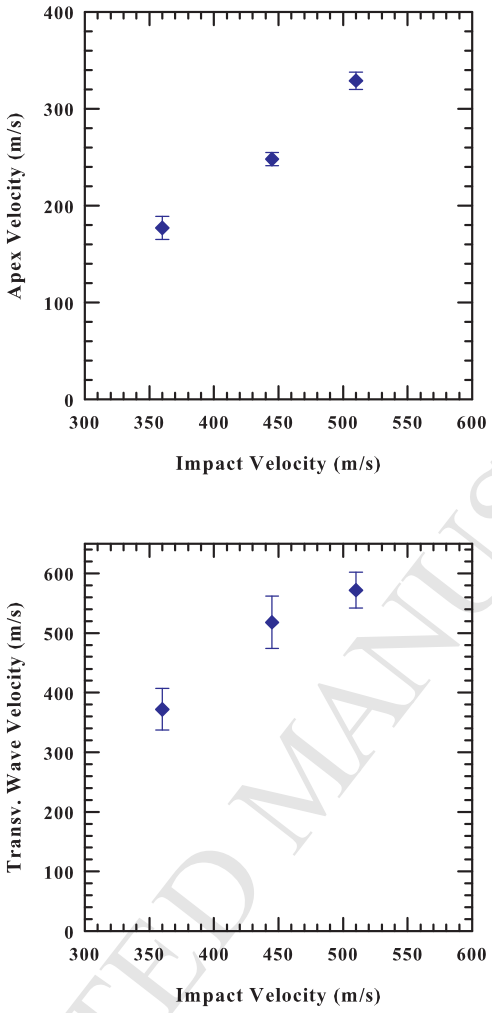

Figure 17: a) Early-time average apex velocity for different impact velocities b) Average transverse wave velocity.

and apex height (displacement) are readily calculated.

The solid lines in Fig. 15 compare the results obtained with this simple model with the experimental results measured with the Imacon camera. Since the agreement is very good for the first $\sim$50 μs it is possible to confirm that the mechanics are well understood, at least for the first part of the fabric response process. Deviations of the model from the test are attributed to failure of yarns, which results in less fabric being carried by the projectile as time advances, that is, the momentum coupling between the projectile and fabric is no longer ideal. More detail concerning the model is provided in Ref. [20].

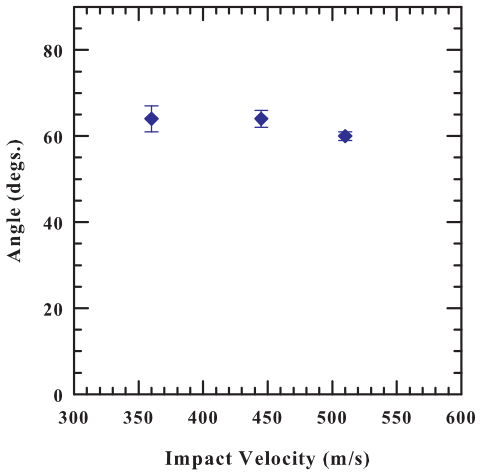

Figure 18: Early-time ($\sim 50\mu s$ *to* $100\mu s$) average apex semiangle for different impact velocities.

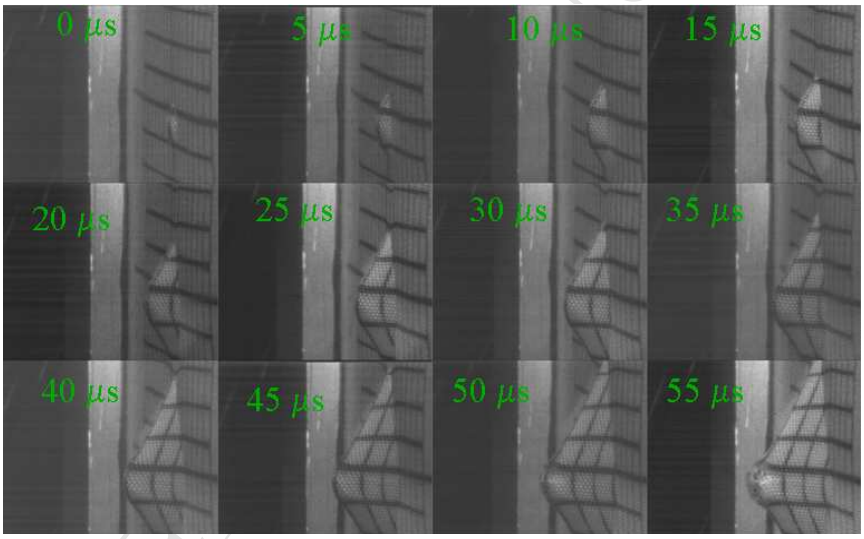

Figure 19: Imacon image of the back of the target for test V2.1-2.

5 Analysis of Phantom's Camera Data

5.1 Late time pyramid motion

Although the Phantom camera was placed primarily to measure the residual velocity of the projectile, it was also used to observe and to measure the deflection of the back of the target (from above). The plane in which the projectile moves was calibrated so that distances in that plane could be measured accurately. This allowed obtaining the motion of the pyramid at late time since the Phantom camera acquired images

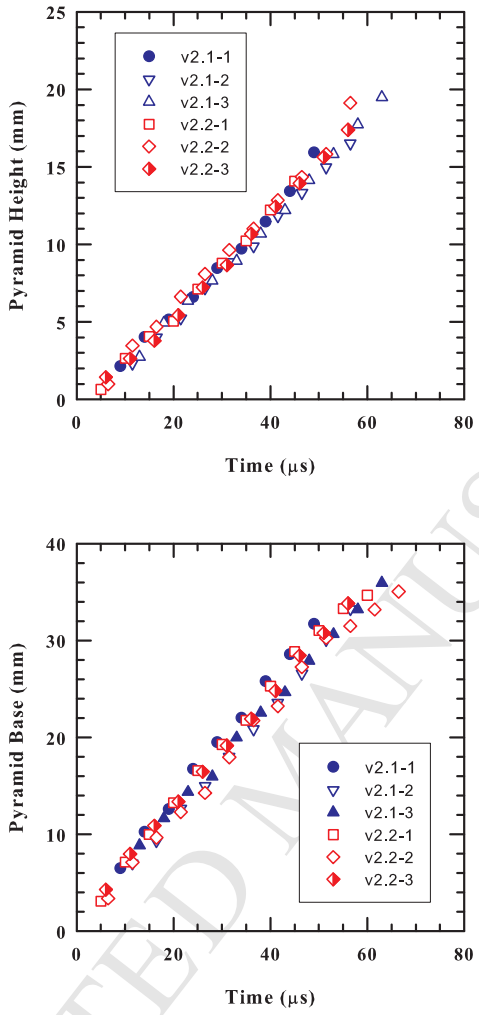

Figure 20: a) Pyramid height vs. time for all the targets shot at velocity V2. b) Pyramid base vs. time for the same targets

up to 3000 μs after the impact. At some point in time ($\sim$ 500 μs) it becomes difficult to follow the base of the pyramid because of complex boundary effects due to the frame. On the other hand, following the apex until maximum deflection was relatively straightforward.

Figure 21 is an example of a sequence of images obtained with the Phantom camera. This camera provides hundreds of images but only six of them are shown here. These cameras allow observation of the whole deflection process and complement the information provided by the Imacon camera.

Figure 22 shows the histories of the apex of the pyramid for impact velocities V1=360 m/s and V2=500 m/s. As discussed in Section 4.2, failure and exit of the

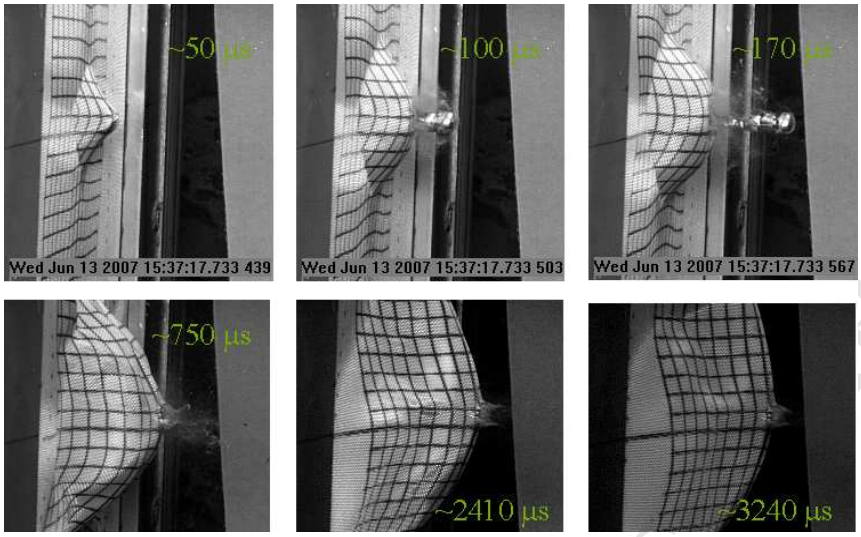

Figure 21: Phantom image sequence of the back of the target for test V2.1-2 (500 m/s).

projectile occurs in the first 50-60 μs after impact; therefore, even if the target fails, deflection continues for another 2000 μs, as observed in Fig. 22(b). The kinetic energy acquired by the fabric is being transferred to strain energy. The maximum deflection is ∼80 mm for the low velocity impact and is smaller for V2: ∼60 mm for high velocity impact. This result is consistent with the results presented in Fig. 9 for the NiCr wire.

6 Conclusions

The objective of this work was to gain understanding of the fundamental mechanisms coming into play in fabrics under ballistic impact. It was decided that measuring the strains during ballistic impact was of major importance to accomplish that objective. Several techniques were tried but the only one that provided a consistent strain measurement was the NiCr wire technique.

It was found in [1] that by weaving a NiCr wire into the fabric it was possible to record the voltage variation due to the strain in the wire. The NiCr wire analysis was supported by high-speed videos, and very-high-speed photography, as well as X-rays. Although the set-up of the tests was involved due to the numerous diagnostic techniques utilized, the combination of all the techniques provided a global picture of the penetration event.

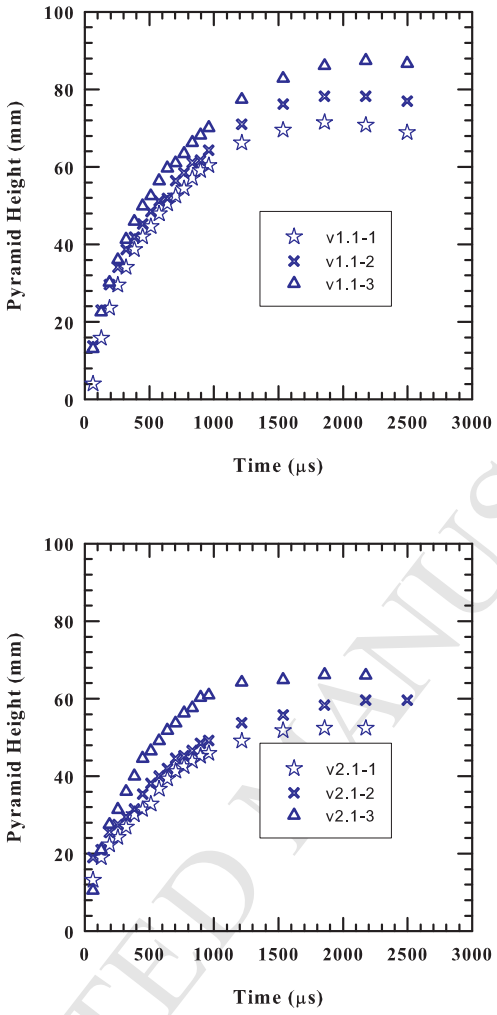

Figure 22: Pyramid height (apex position) history for impacts at velocities a) V1 b) V2.

An energy balance, based on the strains measured with the NiCr wires, was performed at maximum deflection and at failure. The energy balance suggests that during penetration most of the energy goes into straining fibers and into kinetic energy of the fabric. We found from the energy balance analysis that friction does not seem to be a dissipating mechanism, but we believe that it is an effective way of transmitting strain from yarn to yarn. A momentum balance confirms that the fundamental mechanism is well understood.

The NiCr wire also allowed an estimate for the time of failure of each of the layers. The failure times were consistent with the images taken with the Imacon and Phantom cameras.

It is the first time, as far as the authors know, that local and global strains of yarns have been directly obtained (measured) from experimentation. It is also the first time that a detailed balance has been performed on how the energy is partitioned at the yarn level. All of these provide a consistent picture of the penetration phenomena.

References

[1] S. Chocron, K. Ranjan Samant, A. E. Nicholls, E. Figueroa, J. D. Walker, and C. E. Anderson, Jr. Measurement of strain in fabrics under ballistic impact with embedded nichrome wires. Part I: Technique. Accepted in the Int. J. Impact Engng., Jan 2009, doi:10.1016/j.ijimpeng.2009.04.004.

[2] J. C. Smith, F. L. McCrackin, and H. F. Schiefer. Stress-Strain Relationships in Yarns Subjected to Rapid Impact Loading: Part V: Wave Propagation in Long Textile Yarns Impacted Transversely. *Textile Research Journal*, 28(4):288–302, 1958.

[3] D. Roylance and Su-Su Wang. Penetration mechanics of textile structures. Technical Report Natick/TR-80/021, US Army, Natick Research and Development Command, 1979. Contract number DAAG17-76-C-0013.

[4] P. M. Cunniff. *Assessment of Small Arms (ball round) Body Armor Performance, Proc. of 18th International Symposium on Ballistics.* Technomic Publishing Co., Inc., Lancaster, PA, 1999. (W.G. Reinecke, Ed.), pp. 806-813.

[5] P. M. Cunniff. *Decoupled Response of Textile Body Armor, Proc. of 18th International Symposium on Ballistics.* Technomic Publishing Co., Inc., Lancaster, PA, 1999. (W.G. Reinecke, Ed.), pp. 814-821.

[6] P. M. Cunniff. *The V50 Performance of Body Armor Under Oblique Impact, Proc. of 18th International Symposium on Ballistics.* Technomic Publishing Co., Inc., Lancaster, PA, 1999. (W.G. Reinecke, Ed.), pp. 829-836.

[7] P. M. Cunniff. *The Performance of Poly(Para-Phenylene Benzoxazole)(PBO) Fabric for fragmentation Protective Body Armor, Proc. of 18th International Symposium on Ballistics.* Technomic Publishing Co., Inc., Lancaster, PA, 1999. (W.G. Reinecke, Ed.), pp. 837-844.

[8] P. M. Cunniff. A Semiempirical Model for the Ballistic Impact Performance of Textile-Based Personnel Armor. *Textile Research Journal*, 66(1):45–58, 1996.

[9] P. M. Cunniff. An Analysis of the System Effects in Woven Fabrics Under Ballistic Impact. *Textile Research Journal*, 62(9):495–509, 1992.

[10] W. R. Novotny, E. Cepus, A. Shahkarami, R. Vaziri, and A. Poursartip. Numerical investigation of the ballistic efficiency of multi-ply fabric armours during the early stages of impact. *Int. J. Impact Engng.*, 34:71–88, 2007.

[11] D. Roylance, P. Chammas, J. Ting, H. Chi, and B. Scott. Numerical modeling of fabric impact. In *Proceedings of the National Meeting of the American Society of Mechanical Engineers, San Francisco, October 1995*. ASME, 1995.

[12] Y. Duan, M. Keefe, T.A. Bogetti, and B.A. Cheeseman. Modeling friction effects on the ballistic impact behavior of a single-ply high-strength fabric. *Int. J. Impact Engng.*, 31:996–1012, 2005.

[13] A. Shahkarami and R. Vaziri. A continuum shell finite element model for impact simulation of woven fabrics. *Int. J. Impact Engng.*, 34:104–119, 2007.

[14] G.R. Johnson, S.R. Beissel, and P.M. Cunniff. *A computational model for fabrics subjected to ballistic impact*. Technomic Publishing Co., Inc., Lancaster, PA, 1999. (W.G. Reinecke, Ed.), pp. 962-969.

[15] B. Gu. Analytical modeling for the ballistic perforation of planar plain-woven fabric target by projectile. *Composites-B*, 34(4):361–371, 2003.

[16] J. Walker. *Constitutive Model for fabrics with explicit static solution and ballistic limit*. Technomic Publishing Co., Inc., Lancaster, PA, 1999. (W.G. Reinecke, Ed.), pp. 1231-1238.

[17] P. K. Porwal and S. L. Phoenix. Modeling system effects in ballistic impact into multi-layered fibrous materials for soft body armor. *International Journal of Fracture*, 135(1-4):217–249, 2005.

[18] Y. Duan, M. Keefe, T.A. Bogetti, B.A. Cheeseman, and B. Powers. A numerical investigation of the influence of friction on energy absorption by a high-strength fabric subjected to ballistic impact. *Int. J. Impact Engng.*, 32:1299–1312, 2006.

[19] J. P. F. Broos, M. J. van der Jagt-Deutekom, and M. J. van der Voorde. *Ballistic protection of fragment vests against IED threats*. Technomic Publishing Co., Inc., Lancaster, PA, 2008. (S. Bless, J. Walker, Ed.), pp. 527-534.

[20] C. E. Anderson, Jr. and S. Chocron. Experimental results and a simple theory for the early deflection-time history of a ballistic fabric. 16th APS Topical Conf. Shock Waves in Condensed Matter, Nashville, TN, 28 June-3 July 2009.